# Controllable copper deficiency in Cu2−xSe nanocrystals with tunable localized surface plasmon resonance and enhanced chemiluminescence

**ARTICLE** *in* NANOSCALE · JULY 2014

Impact Factor: 7.39 · DOI: 10.1039/c4nr02294g · Source: PubMed



**4 AUTHORS**, INCLUDING:

Mingxuan Gao
Southwest University in Chongqing
**16** PUBLICATIONS **201** CITATIONS
SEE PROFILE

Cheng Zhi Huang
xx
**262** PUBLICATIONS **5,132** CITATIONS
SEE PROFILE

Nanoscale

PAPER

View Article Online
View Journal | View Issue



Cite this: *Nanoscale*, 2014, **6**, 10289

# Controllable copper deficiency in $Cu_{2-x}Se$ nanocrystals with tunable localized surface plasmon resonance and enhanced chemiluminescence†

Shao Qing Lie,[a] Dong Mei Wang,*[a] Ming Xuan Gao[a] and Cheng Zhi Huang*[ab]

Copper chalcogenide nanocrystals (CuCNCs) as a type of semiconductor that can also act as efficient catalysts are rarely reported. Herein, we study water-soluble size-controlled $Cu_{2-x}Se$ nanocrystals (NCs), which are copper deficient and could be prepared by a redox reaction with the assistance of surfactants. We found them to have strong near-infrared localized surface plasmon resonance (LSPR) properties originating from the holes in the valence band, and also catalytic activity of more than a 500-fold enhancement of chemiluminescence (CL) in a luminol–$H_2O_2$ system. Investigations into the mechanisms behind these results showed that the high concentration of free carriers in $Cu_{2-x}Se$ NCs, which are derived from their high copper deficiencies that make $Cu_{2-x}Se$ NCs both good electron donors and acceptors with high ionic mobility, could greatly enhance the catalytic ability of $Cu_{2-x}Se$ NCs to facilitate electron-transfer processes and the decomposition of $H_2O_2$ into $OH^{\cdot}$ and $O_2^{\cdot-}$, which are the commonly accepted key intermediates in luminol CL enhancement. Thus, it can be concluded that controllable copper deficiencies that are correlated with their near-infrared LSPR are critically responsible for the effective catalysis of $Cu_{2-x}Se$ NCs in the enhanced CL.

Received 29th April 2014
Accepted 26th June 2014

DOI: 10.1039/c4nr02294g

www.rsc.org/nanoscale



## Introduction

As an important family of semiconductor nanomaterials, CuCNCs have attracted attention recently due to their specific optical[1–4] and optoelectronic properties.[5–7] For example, copper selenide NCs have been intensively studied and widely used in solar cells,[8] optical filters,[9] and super ionic conductors[10] due to their various phases and structural forms, such as stoichiometric $Cu_2Se$, $Cu_3Se_2$, CuSe, and $CuSe_2$ NCs, as well as non-stoichiometric $Cu_{2-x}Se$ NCs.[11–13] As a p-type semiconductor with electron-ionic conductivity and a direct/indirect band gap of 2.2/1.4 eV,[14] non-stoichiometric $Cu_{2-x}Se$ NCs are particularly suitable for solar light-sensitive photocatalysts.[15]

Current investigations focus on the strong near-infrared (NIR) absorption of the cation-deficient $Cu_{2-x}Se$ NCs, proving that the LSPR originates from the high density of holes in the valence band.[16–18] Different from that of noble metal NCs,[19–21] the NIR-LSPR of $Cu_{2-x}Se$ NCs can be easily engineered, by changing the materials' composition, temperature, or phase transitions,[22] which can then open up new opportunities in sensing,[23] imaging,[24,25] photothermal therapy,[26,27] and plasmonic solar cells.[28,29] Thus, a lot of effort has been devoted to achieve fine-tunability of the LSPR properties of CuCNCs,[14,30–33] providing significant further information on the fundamentals and technological potential about the NIR-LSPR of $Cu_{2-x}Se$ NCs.

It is well known that defects, such as oxygen vacancies and step edges, which have been proposed as participating in chemical catalytic reactions,[34,35] are the most reactive sites on the surfaces of metal oxides, since the defects can bind adsorbates more strongly than normal sites to assist in their dissociation. For example, oxygen vacancies are involved in electrochemical oxygen reduction reactions as their charged nature may control band-bending and thus electron–hole pair separation, greatly enhancing the electrocatalytic activity.[35,36] As an analogy, copper deficiency in $Cu_{2-x}Se$ NCs is important for raising the plasmon resonance, as well as for some electrical properties,[32,37] but few reports have covered the applications of such vacancies for catalysis. Therefore, in this contribution, we investigated the $Cu_{2-x}Se$ NCs involved in catalysis chemistry, by taking the example of luminol chemiluminescence (CL), which is relatively simple but can supply us with a new train of thought for the theoretical understanding of vacancies and allows us to

[a]*Key Laboratory of Luminescence and Real-Time Analytical Chemistry (Southwest University), Ministry of Education, College of Chemistry and Chemical Engineering, Southwest University, Chongqing, 400715, P. R. China. E-mail: wangdm@swu.edu.cn; chengzhi@swu.edu.cn; Fax: +86 23 68367257; Tel: +86 23 68254659*

[b]*College of Pharmaceutical Science, Southwest University, Chongqing 400716, P. R. China*

† Electronic supplementary information (ESI) available: Experimental section and additional figures for XRD, XPS, UV absorption, chemiluminescent spectra, SEM and TEM images. See DOI: 10.1039/c4nr02294g

investigate more practical applications such as bioimaging and immunoassay.

With this aim, we developed a new controllable preparation route of $Cu_2Se$ NCs at room temperature, making use of the reaction of selenium nanoparticles as a template[38] with copper sulfate solution, and found that the available copper deficient $Cu_{2-x}Se$ NCs can induce more than a 500-fold CL enhancement in the typical luminol–$H_2O_2$ system. The observed enhancement effect is unusual and better than most of the reported NCs,[39] which, as we identify herein, is closely related to the unique electronic structure since the copper deficiency in $Cu_{2-x}Se$ NCs markedly supports the increase in free carrier concentration and mobility, which facilitate the electron-transfer process from luminol to $H_2O_2$ and thereby efficiently accelerate the decomposition of $H_2O_2$ to form the active oxygen-related radicals, $OH^{\cdot}$ and $O_2^{\cdot-}$. These active radicals have been commonly identified as the key intermediates that induce CL enhancement.[40] This investigation could lead to valuable new insights into the unique structural characteristics of $Cu_{2-x}Se$ NCs, and could help broaden the application of the novel semiconductor materials in fields, such as sensing, catalysis, and solar cells.

# Experimental

### Apparatus

The UV-vis absorption spectra were measured with a U-3600 spectrophotometer (Hitachi Ltd., Tokyo, Japan). Scanning electron microscopy (SEM) and transmission electron microscopy (TEM) images were captured using an S-4800 scan electron microscope (Hitachi, Japan) and a transmission electron microscope (TEM) (JEM-2100, Japan). Elemental analysis was performed on an ESCALAB 250 X-ray photoelectron spectrometer (Tyoto, Japan). Powder X-ray diffraction (XRD) patterns were obtained using a Shimadzu XRD-7000 and filtered Cu-Ka radiation. Zeta potential and the average hydrodynamic diameters of $Cu_{2-x}Se$ NCs were measured by dynamic laser light scattering (DLS, ZEN3600, Malvern). The ratios of Cu/Se in the nanocrystals and the mass concentration of $Cu_{2-x}Se$ NCs were obtained using inductively couple plasma atomic emission spectrometry (ICPAES).

### Reagents and materials

Luminol and polyvinylpyrrolidone powder (PVP, MW 55 kDa) were commercially obtained from Sigma-Aldrich Co. LLC. (USA). Cetyltrimethyl ammonium bromide (CTAB), sodium dodecyl sulfate (SDS) and copper sulfate ($CuSO_4 \cdot 5H_2O$, 99%) were purchased from Sinopharm Chemical Reagent Co. Ltd. (Shanghai, China). Selenium dioxide ($SeO_2$, 99.9%) was obtained from Aladdin Chemistry Co. Ltd. (Shanghai, China). Polystyrene sulfonate (PSS, MW 70 kDa) and vitamin C (Vc) were purchased from Alfa Aesar Co. Ltd. (MA, USA). All chemicals were used as received without further purification and dissolved in doubly distilled water (18.2 MΩ).

### Synthesis of $Cu_{2-x}Se$ NCs

1.6 ml 10 mg $ml^{-1}$ PSS and 5.5 ml water were added to a round-bottomed flask, and then 0.1 ml 0.2 M $SeO_2$ and 0.3 ml 0.4 M Vc were added successively. After 10 min, a mixed solution of 0.1 ml 0.4 M $CuSO_4 \cdot 5H_2O$ and 0.4 ml 0.4 M Vc were added under vigorous stirring, in which Vc reduced $Cu^{2+}$ to $Cu^{+}$. The resultant mixture was allowed to proceed under vigorous stirring at 30 °C until a green solution was obtained in 10 h, indicating that PSS-stabilized $Cu_{2-x}Se$ NCs was produced. The products obtained were purified through a 10 kDa dialysis membrane for 1 day with 6 changes of distilled water in order to remove the small molecules and centrifugation if necessary to remove the large molecules. The products were finally stored in a 4 °C refrigerator. It was found that the products obtained are stable within 1 month (Fig. S1, ESI†). Other surfactant-stabilized $Cu_{2-x}Se$ NCs were synthesized also following the same procedures with a reaction time of 3 h for CTAB, or 10 h for SDS or PVP, respectively. The molar extinction coefficient of all the $Cu_{2-x}Se$ NCs were calculated on the absorbance peak wavelength with various concentrations.[26]

### Chemiluminescence measurements

The CL spectra and the dynamic CL intensity–time profiles of PSS–$Cu_{2-x}Se$ NCs-enhanced luminol CL were measured with an ultra-weak BPCL luminescence analyzer (Institute of Biophysics, Chinese Academy of Sciences, Beijing, China) using the static model in a 3 ml quartz cuvette. Before the CL signals were recorded, the analyzer was always first run for half an hour to ensure good reproducibility. The dynamic profiles were displayed and integrated for a 0.2 s interval at −750 V. The CL spectra were obtained through a series of high-energy cut-off filters (wavelengths from 230 to 640 nm), which were placed between the flow CL cell and the photomultiplier of the analyzer. 250 μl of luminol solution was quickly injected by a microliter syringe into a mixture premixed with 100 μl of $H_2O_2$ and 100 μl of PSS–$Cu_{2-x}Se$ NCs in the cuvette. When investigating the influence of different radical scavengers on luminol–$H_2O_2$ CL in the presence of $Cu_{2-x}Se$ NCs, 100 μl of radical scavengers with different concentrations were first introduced into the mixture of $H_2O_2$ and $Cu_{2-x}Se$ NCs following the same experimental procedures as described above. $(I_0 - I)/I_0 \times 100\%$ was used to calculate CL percent inhibition, and the $I_0$ or $I$ were the CL intensities in the absence or presence of radical scavengers, respectively.

# Results and discussion

### A route to prepare $Cu_{2-x}Se$ NCs with controllable sizes

Template-directed synthesis was identified as an effective and facile strategy to prepare CuCNCs.[38,41–43] Although this approach usually requires a relatively low temperature, or even room temperature, the as-prepared CuCNCs have weak LSPR absorption. Considering that surfactants can influence both the morphology of $Cu_{2-x}Se$ NCs related to the LSPR frequency[32] and the catalytic activity of NCs,[44,45] we herein developed a template-directed synthesis route to prepare $Cu_{2-x}Se$ NCs with

 

controllable sizes by introducing four kinds of water-soluble surfactants, including cations (CTAB), anions (SDS), anionic polymer (PSS), non-ionic polymer (PVP).

The built-up simple reaction route was composed of three steps (Fig. 1). First, Vc was employed to reduce $SeO_2$ into orange Se NCs (Fig. 1a) in the presence of the surfactants. Second, $Cu_2Se$ NCs were formed with the addition of $Cu^+$ (mixture solution of $CuSO_4$ and Vc) into Se NCs, since $Cu^+$ can catalyze $Se^0$ into $Se^{2-}$ and $Se^{4+}$,[38] during which the colour of solution changed from orange to brown (Fig. 1b). Finally, the as-formed $Cu_2Se$ NCs gradually transformed into $Cu_{2-x}Se$ NCs with a color change to green through a phase transformation process promoted by air exposure and the unreacted oxidants (Fig. 1c).[10] The formation of the orange Se NCs in the first step can be identified by the TEM and HR-TEM images (Fig. 2a–c), and these Se NCs had a spacing of 0.39 nm, corresponding to the (100) planes.[46] Fig. 2 also clearly shows the formation of $Cu_2Se$ NCs and $Cu_{2-x}Se$ NCs, wherein HR-TEM images demonstrate the phase transformation from $Cu_2Se$ NCs with the measured spacings of 3.4 Å and 2.3 Å, corresponding to the (060) and (090) planes to $Cu_{2-x}Se$ NCs with the measured spacings of 2.4 Å and 2.1 Å, corresponding to the (012) and (220) planes.[10,47]

As the TEM images in Fig. 3 show, after the three steps, the as-prepared particles were quite monodispersed and uniform, and their size could be adjusted from 14.5 nm to 52.0 nm by changing the surfactants. Powder X-ray diffraction (XRD) identified that the as-prepared $Cu_{2-x}Se$ NCs were a cubic berzelianite phase with a well-defined crystalline form (Fig. S2, ESI†), while the X-ray photoelectron spectroscopic (XPS) measurements (Fig. S3, ESI†) also identified the $Cu_{2-x}Se$ phase with the binding energies of 932.30 eV for Cu $2p_{3/2}$ and 54.84 eV for Se 3d. The Cu $2p_{3/2}$ peak appearing at 932.30 eV corresponds to either $Cu^0$ or Cu(I). A noticeable phenomenon is that an asymmetric peak shape toward high binding energies appeared, indicating the presence of Cu(II).[48] In other words, the available

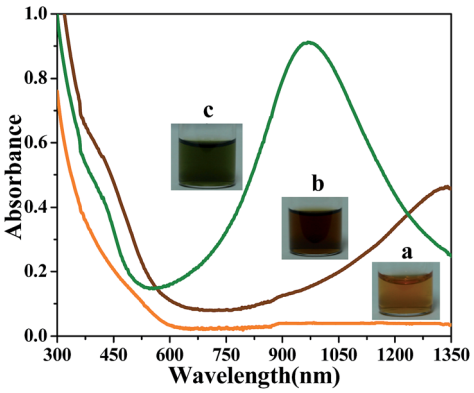


Fig. 1 Step-by-step absorption spectra and visual observation of the formation of $Cu_{2-x}Se$ NCs stabilized by PSS. (a) The Se NCs were obtained with the reaction of Vc and $SeO_2$ in 10 min in the first step. (b) The $Cu_2Se$ NCs obtained after the cuprous ion was mixed with Se NCs in 0.5 h in the second step. (c) The $Cu_{2-x}Se$ NCs obtained with the extended reaction time of $Cu_2Se$ NCs being oxidized in the third step. The insets were the solution images of Se NCs, $Cu_2Se$ NCs and $Cu_{2-x}Se$ NCs, respectively.

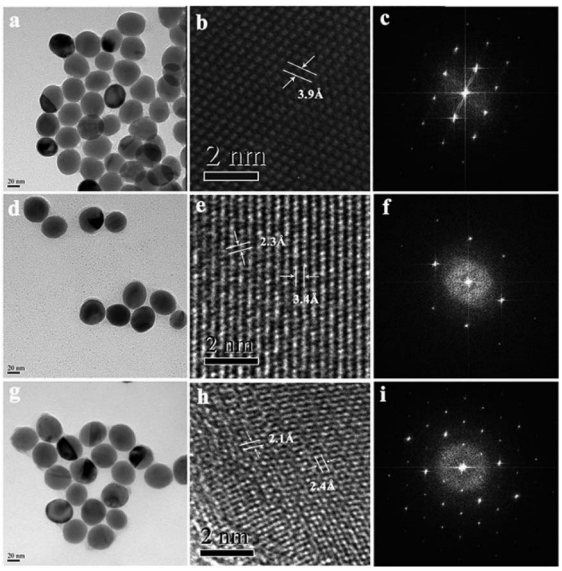


Fig. 2 TEM images to visualize the formation of Se NCs, $Cu_2Se$ NCs and $Cu_{2-x}Se$ NCs stabilized by PSS. TEM images (a, d, and g), HR-TEM images (b, e, and h), and corresponding numerical diffractogram (FFTs, c, f, and i) of Se NCs (a, b, and c), $Cu_2Se$ NCs (d, e, and f), and $Cu_{2-x}Se$ NCs (g, h, and i), respectively.

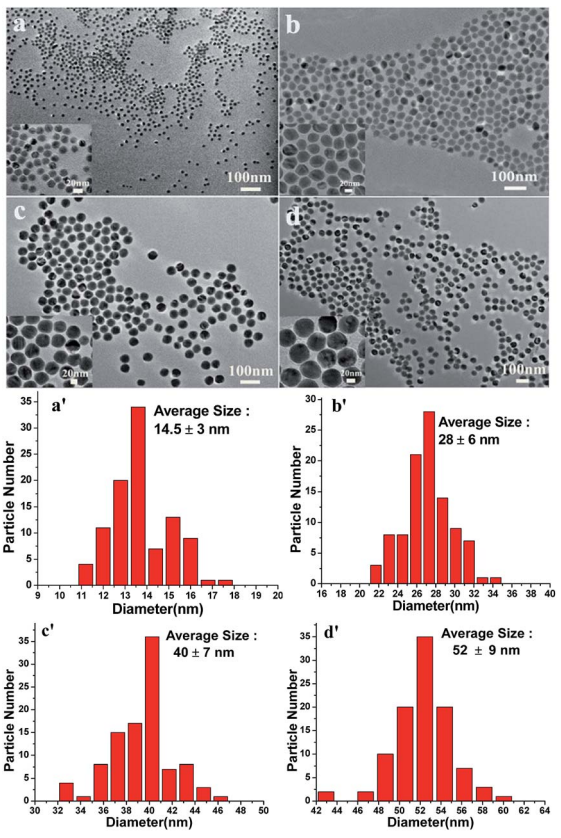


Fig. 3 Surfactant-dependent sizes of $Cu_{2-x}Se$ NCs as shown by TEM images. $Cu_{2-x}Se$ NCs were coated by CTAB (a and a′), SDS (b and b′), PSS (c and c′) and PVP (d and d′), respectively. Size distributions are obtained by counting 100 particles of each sample.

final products were nonstoichiometric $Cu_{2-x}Se$ with a high copper deficiency.[49]

The monodispersed growth of $Cu_{2-x}Se$ NCs with size tunability could be attributed to the surfactant and the size-focusing effect,[32] as the size of the nanoparticles could be restricted to a certain range with the changing concentration of different surfactants (Fig. S4, ESI†). Therefore, it is suggested that surfactants may somehow complex selenium and then copper ions in the reaction.

In the first step, the type of the surfactants may be essential in the synthesis of monodispersed size-tunable Se NCs (Table S1, ESI†). During the formation of Se NCs, the size of Se NCs is controlled by the surfactants, following a burst of nucleation at a constant volumetric growth rate.[32] CTAB and SDS are much smaller molecules than PVP or PSS, thus allowing a larger mobility and reactivity of the surfactant–ion system. This could also decrease the barrier for nucleation, favoring, in the case of CTAB- and SDS-complexed ions, many more nuclei, and hence smaller growth. Furthermore, it should be considered that PVP and PSS are polymeric molecules, and therefore offer many anchoring groups to selenium with respect to CTAB or SDS. Therefore, the size of Se NCs obtained by CTAB or SDS is relatively smaller than that by PSS or PVP.

In the second step, during which cuprous ion reacts with the templated Se NCs,[50] the formation of $Cu_2Se$ may be controlled by different rates of ionic diffusion induced by the different surfactants. The oxygen groups in SDS or PSS or the PVP surfactant have a trend to coordinate to cuprous cations, which slows down the diffusion to the nucleation.[51] Therefore, while the formation rates of the product prepared by the different surfactants are different, they do not induce large changes of size from Se NCs to $Cu_2Se$ NCs, as shown by the TEM image (Fig. 2) and the DLS measurement (Table S1, ESI†).

In the third step, the phase transformation from $Cu_2Se$ to $Cu_{2-x}Se$ is observed by the colour change and the strong absorption in NIR (Fig. 1c), where air exposure produces an oxidation of the nanoparticle surface, which is also supported by the XRD pattern (Fig. S5, ESI†),[49] followed by the creation of a potential along the particle diameter, which promotes a diffusion of copper ions from the inner core to the surface. It is found that the NCs preserve their size and shape in the transformation (Fig. 2), which is a result similar to the reported chemical transformation starting from $Cu_2Se$ nanocrystals.[10,47]

### High copper deficiency of $Cu_{2-x}Se$ NCs

The available nonstoichiometric $Cu_{2-x}Se$ NCs with high copper deficiency could be well-dispersed in water, with an absorption from the UV to the NIR region (Fig. 4a). The absorption in the UV-vis region below 500 nm has been ascribed to the direct band gap, and the one in NIR region should be the LSPR.[4,7,26] It is known that the NIR-LSPR depends on the relatively high carrier (holes) concentration and sizes of the nanocrystals.[22,32] Here, the NIR-LSPR is easily tuned by changing the surfactants and reaction time (Fig. 4b). Within the same reaction time, different surfactants, such as PVP, SDS, and PSS, can be used to control the LSPR frequency of $Cu_{2-x}Se$ NCs, which have strong

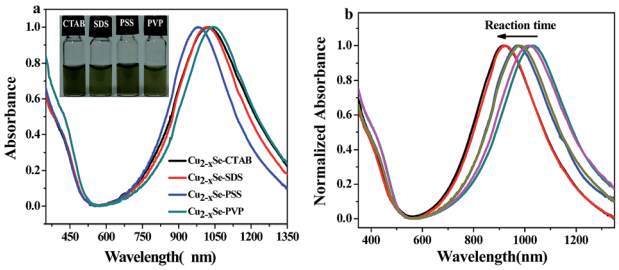


Fig. 4 NIR-LSPR absorption spectra of $Cu_{2-x}Se$ NCs. (a) The absorption spectra of crystalline $Cu_{2-x}Se$ NCs coated by CTAB (30 °C, 3 h), SDS (30 °C, 10 h), PSS (30 °C, 10 h), and PVP (30 °C, 10 h) with sizes of 14.5 nm, 28 nm, 40 nm, and 52 nm, respectively. Different surfactants capping $Cu_{2-x}Se$ NCs showed different absorption bands, characterized at 1025 nm, 1020 nm, 980 nm, and 1040 nm with molar extinction coefficients of $3.8 \times 10^8$ $M^{-1}$ $cm^{-1}$, $2.2 \times 10^9$ $M^{-1}$ $cm^{-1}$, $4.7 \times 10^9$ $M^{-1}$ $cm^{-1}$, and $1.2 \times 10^{10}$ $M^{-1}$ $cm^{-1}$, respectively. The inset was the solution image of $Cu_{2-x}Se$ NCs coated by CTAB, SDS, PSS, and PVP, respectively. (b) With the reaction time going from 8 h to 12 h at 30 °C, the absorption spectra of crystalline PSS–$Cu_{2-x}Se$ are blue-shifted.

absorption peaks centered at 1045 nm, 1020 nm and 980 nm. In addition, the LSPR frequency of $Cu_{2-x}Se$ NCs only weakly depends on the size while relying more on the electric charge of the surfactants. As the electric charge of the surfactants are more negative (Table S1, ESI†), $Cu_{2-x}Se$ NCs show a more significant blue-shift in LSPR absorption with a Cu/Se ratio of 1.6 ($x = 0.4$).

It was also found that CTAB could accelerate the phase transformation from the $Cu_2Se$ NCs to the $Cu_{2-x}Se$ NCs with a Cu/Se ratio of 1.2 ($x = 0.8$) within 3 h. Compared with other surfactants, CTAB can make $Cu_{2-x}Se$ NCs have a higher copper deficiency, but cannot unexpectedly cause any blue shift in the LSPR of $Cu_{2-x}Se$ NCs,[17] which could be ascribed to the more positive charge of CTAB than others. Therefore it is suggested that the positive charge on the surface of $Cu_{2-x}Se$ NCs may trap free holes and thereby reduce the effective free carrier concentration, which is similar to oleic acid as a Lewis acid with the ability to accept electrons.[32] On the contrary, the negative charge on the surface of $Cu_{2-x}Se$ NCs highly increases the charge carrier density, which leads to a blue-shift of LSPR. Moreover, the molar extinction coefficient of $Cu_{2-x}Se$ NCs show a strong size dependence, and as the size increases the molar extinction coefficient increases.

Furthermore, it is easy to control the NIR-LSPR band of $Cu_{2-x}Se$ NCs by extending the reaction time in the presence of PSS (Fig. 4b). Therefore, we can adjust the copper deficiency of $Cu_{2-x}Se$ NCs since the blue shift of NIR-LSPR indicates an increasing copper deficiency,[17,47] and thus the copper deficiency is controllable. Moreover, the LSPR features induced by the copper deficiency of the available $Cu_{2-x}Se$ NCs are greatly dependent on the surrounding medium, and it is found that the NIR absorption of $Cu_{2-x}Se$ NCs is red-shifted with the increasing refractive index of the surrounding solvent media (Fig. S6, ESI†), which is identical to the LSPR absorption features of noble metal nanocrystals such as gold and silver nanocrystals.[21,52]

 

### Copper deficiency of $Cu_{2-x}Se$ NCs induced strong CL enhancement

In order to identify the excellent catalytic ability related to the high copper deficiency of $Cu_{2-x}Se$ NCs, we use the well-known luminol–$H_2O_2$ CL system as an example. Fig. 5 shows the highly catalytic performance of $Cu_{2-x}Se$ NCs coated by PSS (PSS–$Cu_{2-x}Se$ NCs), in comparison with the dynamic CL intensity–time profiles of luminol–$H_2O_2$ system in the absence and presence of PSS–$Cu_{2-x}Se$ NCs. It can be seen that PSS–$Cu_{2-x}Se$ NCs can greatly enhance the CL intensity of luminol, as high as up to 530 times, compared to the weak luminol CL oxidized only by $H_2O_2$ in alkaline medium (Fig. 5a). This strongly enhanced CL effect is the best one among the reported nanocatalysis.[33] Similar to other nanocatalysts, the catalytic activity of PSS–$Cu_{2-x}Se$ NCs is closely related to the pH and the concentrations of the reaction reagents. The optimal condition was $2.0 \times 10^{-4}$ M luminol in NaOH solution (pH 11.1), 70.0 pM PSS–$Cu_{2-x}Se$ NCs, and 22.2 μM $H_2O_2$, respectively (Fig. S7, ESI†).

In such a case, it is necessary to clarify whether the observed catalytic effect of PSS–$Cu_{2-x}Se$ NCs is derived from the unreacted reagents used in the synthetic processes. Fig. 5b shows that there are some degree of CL enhancement by $Cu^{2+}$, PSS, or the mixture of $Cu^{2+}$ and PSS solution with the same concentrations as the synthetic procedures, but the enhanced degrees are greatly weaker than that of PSS–$Cu_{2-x}Se$ NCs under the same conditions. Furthermore, the as-prepared PSS–$Cu_{2-x}Se$ NCs were subjected to dialysis (24 h) and centrifugation (10 000 rpm, 10 min) to remove the residual $Cu^{2+}$ or PSS species. Hence, the possibility of the CL enhancement effect from concomitant species such as $Cu^{2+}$ or PSS can be excluded, and also from the intrinsic catalytic property of the intact PSS–$Cu_{2-x}Se$ NCs.

The CL spectra of luminol–$H_2O_2$, both in the presence and absence of PSS–$Cu_{2-x}Se$ NCs, were acquired (Fig. S8, ESI†). It is clearly indicated that the maximum emission is ~440 nm, revealing that the luminophors in both cases are the excited-state 3-aminophthalate anions (3-APA*), in agreement with the reported nanocatalysis.[32,53,54] In addition, the SEM and TEM measurements (Fig. S9, ESI†) show no significant differences or changes in the size, and shape for PSS–$Cu_{2-x}Se$ NCs before or after the CL reaction, so we can conclude that the NCs act as a catalyst to enhance luminol CL.

In order to identify the catalytic process of PSS–$Cu_{2-x}Se$ NCs during the CL process, further investigations are necessary in terms of the key oxygen-related radical intermediates induced luminescence enhancement, such as quenching experiments of different active oxygen radical scavengers on the CL intensity. Therefore, the effects of Vc (a common scavenger of oxygen-related radicals), thiourea (a scavenger of OH· radicals), superoxide dismutase (SOD, a scavenger of $O_2^{\cdot-}$ radicals) and $NaN_3$ (a scavenger of $^1O_2$) were measured. The results indicate that Vc, thiourea, and SOD all decreased the CL remarkably, but no CL inhibition occurred for $NaN_3$ (Fig. S10, ESI†), suggesting that OH· and $O_2^{\cdot-}$, but not $^1O_2$, were produced during the CL process. In other words, OH· and $O_2^{\cdot-}$ did contribute to the observed CL. Apart from the breakdown of $H_2O_2$, a small fraction of the above radicals could come from the dissolved oxygen of the reagent solutions, as there were some changes in average CL intensity CL signal (less than 20% change) when $N_2$ was bubbled into the reactant solutions for a few minutes before the CL reaction.

Furthermore, the room temperature electron spin resonance (ESR) technique, which was used to detect oxygen-related radicals because of their short lifetime, was explored, wherein 5,5-dimethyl-1-pyrroline-*N*-oxide (DMPO) was used as a specific target molecule to determine OH·. As shown in Fig. 6a, the DMPO/OH· adduct signal intensity of the ESR spectra in the presence of PSS–$Cu_{2-x}Se$ NCs is clear and much stronger than that without NCs, indicating that PSS–$Cu_{2-x}Se$ NCs have excellent catalytic activity to accelerate the decomposition of $H_2O_2$ to generate a high yield of OH· on their surface. As a specific target molecule of $^1O_2$, 2,2,6,6-tetramethyl-4-piperidine (TEMP) can react with $^1O_2$ to form a stable, ESR-measurable 2,2,6,6-tetramethyl-4-piperidine-*N*-oxide (TEMPO) adduct. However, regardless of the presence or absence of NCs, the signal intensity of TEMPO remains nearly the same in the luminol–$H_2O_2$ system (Fig. 6b), proving no generation of $^1O_2$, identical to the results of the above quenching experiments. In

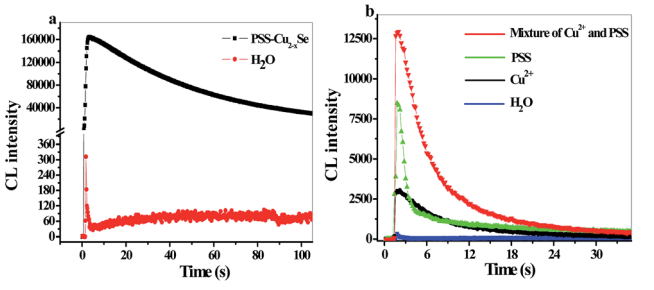


Fig. 5 $Cu_{2-x}Se$ NCs with high copper deficiency ($x \sim 0.4$) induces strong chemiluminescence. Kinetic monitoring on luminol–$H_2O_2$ CL in the presence of (a) PSS–$Cu_{2-x}Se$ NCs, and (b) the reagents including $Cu^{2+}$, PSS, or their mixture used in the synthesis processes. Conditions: luminol, $2.0 \times 10^{-4}$ M; $H_2O_2$, 22.2 μM; PSS–$Cu_{2-x}Se$ NCs, 70.0 pM; $Cu^{2+}$, 5 mM; PSS, 2.0 mg ml.

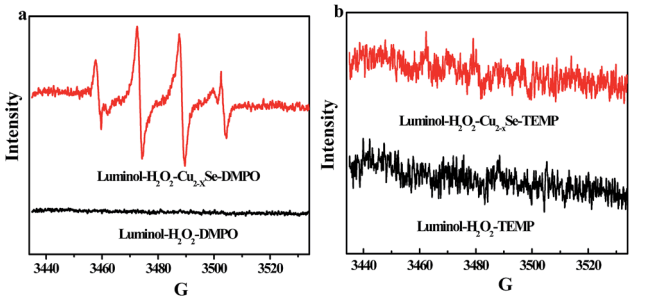


Fig. 6 ESR spectra of (a) DMPO-OH· adduct, and (b) nitroxide radicals generated by the reaction of TEMP probe with $^1O_2$ in luminol–$H_2O_2$ system in the presence (red line) or absence (black line) of PSS–$Cu_{2-x}Se$. Conditions: modulation amplitude, 1.944 G; microwave power, 1.002*e* + 001 mW; receiver gain, 1.00*e* + 005; sweep width, 100.00 G. The ESR measurements were achieved with a Bruker ESP-300E spectrometer operating in the X-band at room temperature.

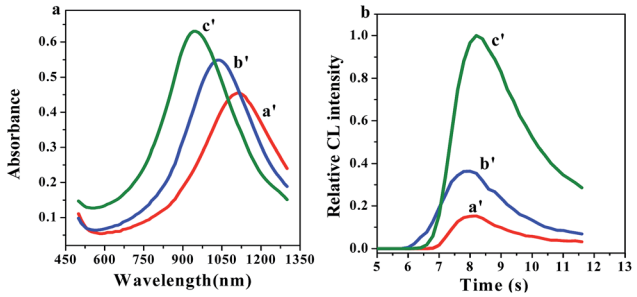


Fig. 7 PSS–$Cu_{2-x}Se$ NCs with different free carrier concentrations and their kinetic monitoring on luminol–$H_2O_2$ CL. (a) Three PSS–$Cu_{2-x}Se$ NCs (a′, b′ and c′) with different absorption spectra were obtained at different reaction times. (b) Kinetic monitoring on luminol–$H_2O_2$ CL in the presence of a′, b′ and c′, respectively. Conditions: luminol, $2.0 \times 10^{-4}$ M; $H_2O_2$, $1 \times 10^{-4}$ M.

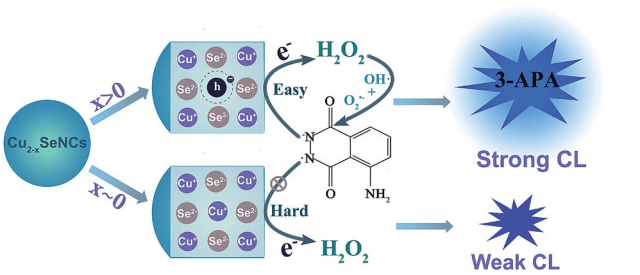


Scheme 1 Illustration of the high performance of $Cu_{2-x}Se$ NCs for luminol–$H_2O_2$ CL system.

fact, $Cu_{2-x}Se$ NCs coated by the other three surfactants (SDS, PVP, and CTAB) can also enhance the CL by at least 500 times (Fig. S11, ESI†). Moreover, it is found that $Cu_{2-x}Se$ NCs ($x \sim 0$) cannot strongly induce an enhancement of CL compared to $Cu_{2-x}Se$ NCs ($x > 0$) (Fig. S12, ESI†). Therefore, the unique structures of $Cu_{2-x}Se$ NCs, especially the high copper deficiencies, play a critical role in their excellent catalytic activity. As shown in Fig. 7, $Cu_{2-x}Se$ NCs with an increasing density of free carriers (holes) induced by copper deficiency show an increase in catalytic activity. It has been reported that the vacancies in the structure would make the charge carrier density increase, and thus enhance the electronic properties.[10] Similarly, the copper deficiency in $Cu_{2-x}Se$ NCs should be responsible for an increase in the charge carrier density, which should induce an enhancement of the catalytic activity on the luminol–$H_2O_2$ CL system.

On the other hand, we tested the spectral changes of $Cu_{2-x}Se$ NCs before and after luminol CL (Fig. 8). As expected, at the beginning, a blue shift of the LSPR peak was observed for $Cu_{2-x}Se$ NCs after the addition of $H_2O_2$, due to the fact that electron transfer occurred from NCs to $H_2O_2$ which confirmed a decrease in the electron density of NCs. Then, when luminol was added to the mixture of NCs and $H_2O_2$, the characteristic LSPR peak of NCs showed some recovery to the original position, revealing that the electrons from luminol were somehow re-injected into NCs. These novel observations confirmed NCs as good electron donors and acceptors to facilitate not only the breakdown $H_2O_2$ to produce oxygen-related radicals, but also electron-transfer processes taking place on the NC surface, similar to the previously reported nanocatalysis.[40] As shown in Scheme 1, the mechanism clearly demonstrates the importance of copper deficiency in making $Cu_{2-x}Se$ NCs facilitate electron-transfer from luminol to $H_2O_2$ and the decomposition of $H_2O_2$ into OH˙ and $O_2^{\cdot-}$.

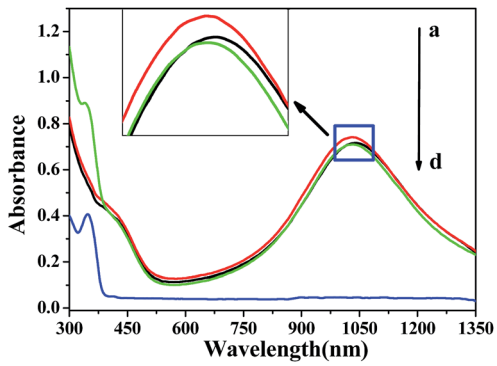


Fig. 8 UV-visible absorption spectra of (a) $H_2O_2$–PSS–$Cu_{2-x}Se$, (b) PSS–$Cu_{2-x}Se$, (c) luminol–$H_2O_2$–PSS–$Cu_{2-x}Se$, and (d) luminol–$H_2O_2$. Final concentrations: luminol, $2.0 \times 10^{-4}$ M; $H_2O_2$, 222 μM. The inset is a local amplification of the absorption diagram from 950 nm to 1110 nm.

Moreover, the possibility that copper ion acts as a catalyst to decompose $H_2O_2$ into OH˙ and $O_2^{\cdot-}$ in alkaline medium[55] should be considered. As our experiment demonstrated the existence of OH˙ and $O_2^{\cdot-}$ contributing to the observed strong CL by oxidizing the luminol as 3-APA*, we supposed that the copper ion on the surface of $Cu_{2-x}Se$ NCs had an important role on increasing the CL signal of the luminol–$H_2O_2$ system. However, with the same copper ion concentration, $Cu_{2-x}Se$ NCs had a stronger catalytic ability than that of free copper ion (Fig. 5). Moreover, the higher free carrier concentrations that $Cu_{2-x}Se$ NCs have, the stronger the CL signal shows $Cu_{2-x}Se$ NCs (Fig. 7). Therefore, it is not only the copper ion but also the copper deficiency that plays a prominent part in the CL enhancement. The copper deficiency in $Cu_{2-x}Se$ NCs is responsible for the formation of the hole, the high free carrier concentration, and the high ionic mobility, which then largely prompts the catalytic ability of $Cu_{2-x}Se$ NCs to decompose $H_2O_2$ and facilitate the electron-transfer processes.

## Conclusions

In summary, we developed a simple method to synthesize $Cu_{2-x}Se$ NCs with different surfactants, wherein the surfactants in the reaction of cuprous and Se NCs not only control the size of $Cu_{2-x}Se$ NCs but also confine carrier (holes) to a certain concentration. Owing to the controllable copper deficiencies, the as-prepared $Cu_{2-x}Se$ NCs have strong NIR-LSPR properties, and excellent catalytic activity of more than 500-fold CL enhancement in a luminol–$H_2O_2$ system, mainly through the commonly accepted OH˙ and $O_2^{\cdot-}$ radicals. The present study

 

displays a new application of $Cu_{2-x}Se$ NCs in CL field, which should be important for gaining a better understanding of the unique structure of copper deficiencies, and to support further research about the proposed NCs currently in progress.

## Acknowledgements

The presented research was financially supported by the National Natural Science Foundation of China (NSFC, 21375109) and the Cultivation Plan of Chongqing Science & Technology Commission for 100 Outstanding Science and Technology Leading Talents.



## Notes and references

1 A. M. Malyarevich, K. V. Yumashev, N. N. Posnov, V. P. Mikhailov, V. S. Gurin, V. B. Prokopenko, A. A. Alexeenko and I. M. Melnichenko, *J. Appl. Phys.*, 2000, **87**, 5.
2 Y. Xie, L. Carbone, C. Nobile, V. Grillo, S. D'Agostino, F. Della Sala, C. Giannini, D. Altamura, C. Oelsner, C. Kryschi and P. D. Cozzoli, *ACS Nano*, 2013, **7**, 7352–7369.
3 I. Kriegel, J. Rodriguez-Fernandez, A. Wisnet, H. Zhang, C. Waurisch, A. Eychmuller, A. Dubavik, A. O. Govorov and J. Feldmann, *ACS Nano*, 2013, **7**, 4367–4377.
4 A. L. Routzahn, S. L. White, L.-K. Fong and P. K. Jain, *Isr. J. Chem.*, 2012, **52**, 983–991.
5 J. J. Loferski, *Mater. Sci. Eng., B*, 1992, **13**, 271–277.
6 J. Choi, N. Kang, H. Y. Yang, H. J. Kim and S. U. Son, *Chem. Mater.*, 2010, **22**, 3586–3588.
7 F. Scotognella, G. Valle, A. Srimath Kandada, M. Zavelani-Rossi, S. Longhi, G. Lanzani and F. Tassone, *Eur. Phys. J. B*, 2013, **86**, 1–13.
8 R. S. Mane, S. P. Kajve, C. D. Lokhande and S.-H. Han, *Vacuum*, 2006, **80**, 631–635.
9 S. T. Lakshmikumar and A. C. Rastogi, *Sol. Energy Mater. Sol. Cells*, 1994, **32**, 7–19.
10 S. C. Riha, D. C. Johnson and A. L. Prieto, *J. Am. Chem. Soc.*, 2011, **133**, 1383–1390.
11 Y. Xie, X. Zheng, X. Jiang, J. Lu and L. Zhu, *Inorg. Chem.*, 2001, **41**, 387–392.
12 A. Jagminas, R. Juškėnas, I. Gailiūtė, G. Statkutė and R. Tomašiūnas, *J. Cryst. Growth*, 2006, **294**, 343–348.
13 K.-H. Low, C.-H. Li, V. A. L. Roy, S. S.-Y. Chui, S. L.-F. Chan and C.-M. Che, *Chem. Sci.*, 2010, **1**, 515–518.
14 S. Deka, A. Genovese, Y. Zhang, K. Miszta, G. Bertoni, R. Krahne, C. Giannini and L. Manna, *J. Am. Chem. Soc.*, 2010, **132**, 8912–8914.
15 T. D. T. Ung and Q. L. Nguyen, *Nanosci. Nanotechnol.*, 2011, **2**, 6.
16 F. Scotognella, G. Della Valle, A. R. Srimath Kandada, D. Dorfs, M. Zavelani-Rossi, M. Conforti, K. Miszta, A. Comin, K. Korobchevskaya, G. Lanzani, L. Manna and F. Tassone, *Nano Lett.*, 2011, **11**, 4711–4717.
17 Y. Zhao, H. Pan, Y. Lou, X. Qiu, J. Zhu and C. Burda, *J. Am. Chem. Soc.*, 2009, **131**, 4253–4261.
18 A. Comin and L. Manna, *Chem. Soc. Rev.*, 2014, **43**, 3957–3975.
19 L. Zhang, C. Z. Huang, Y. F. Li and Q. Li, *Cryst. Growth Des.*, 2009, **9**, 3211–3217.
20 L. Zhang, S. J. Zhen, Y. Sang, J. Y. Li, Y. Wang, L. Zhan, L. Peng, J. Wang, Y. F. Li and C. Z. Huang, *Chem. Commun.*, 2010, **46**, 4303–4305.
21 Y. Liu and C. Z. Huang, *Nanoscale*, 2013, **5**, 7458–7466.
22 J. M. Luther, P. K. Jain, T. Ewers and A. P. Alivisatos, *Nat. Mater.*, 2011, **10**, 361–366.
23 Y. D. Zhu, J. Peng, L. P. Jiang and J. J. Zhu, *Analyst*, 2014, **139**, 649–655.
24 X. Liu, W.-C. Law, M. Jeon, X. Wang, M. Liu, C. Kim, P. N. Prasad and M. T. Swihart, *Adv. Healthcare Mater.*, 2013, **2**, 952–957.
25 X. Liu, C. Lee, W. C. Law, D. Zhu, M. Liu, M. Jeon, J. Kim, P. N. Prasad, C. Kim and M. T. Swihart, *Nano Lett.*, 2013, **13**, 4333–4339.
26 C. M. Hessel, V. P. Pattani, M. Rasch, M. G. Panthani, B. Koo, J. W. Tunnell and B. A. Korgel, *Nano Lett.*, 2011, **11**, 2560–2566.
27 X. Liu, Q. Wang, C. Li, R. Zou, B. Li, G. Song, K. Xu, Y. Zheng and J. Hu, *Nanoscale*, 2014, **6**, 4361–4370.
28 Y. Zhao and C. Burda, *Energy Environ. Sci.*, 2012, **5**, 5564–5576.
29 P. Hu and Y. Cao, *J. Nanopart. Res.*, 2012, **14**, 1–8.
30 P. Huang, Y. Kong, Z. Li, F. Gao and D. Cui, *Nanoscale Res. Lett.*, 2010, **5**, 949–956.
31 X. Liu, X. Duan, P. Peng and W. Zheng, *Nanoscale*, 2011, **3**, 5090–5095.
32 X. Liu, X. Wang, B. Zhou, W.-C. Law, A. N. Cartwright and M. T. Swihart, *Adv. Funct. Mater.*, 2013, **23**, 1256–1264.
33 J. Zhu, Q. Li, L. Bai, Y. Sun, M. Zhou and Y. Xie, *Chem.–Eur. J.*, 2012, **18**, 13213–13221.
34 C. T. Campbell and C. H. F. Peden, *Science*, 2005, **309**, 713–714.
35 F. Cheng, T. Zhang, Y. Zhang, J. Du, X. Han and J. Chen, *Angew. Chem., Int. Ed.*, 2013, **52**, 2474–2477.
36 M. Nolan, S. C. Parker and G. W. Watson, *Surf. Sci.*, 2005, **595**, 223–232.
37 S. C. Riha, D. C. Johnson and A. L. Prieto, *J. Am. Chem. Soc.*, 2010, **133**, 1383–1390.
38 F. X. Rong, Y. Bai, T. F. Chen and W. J. Zheng, *Mater. Res. Bull.*, 2012, **47**, 92–95.
39 W. Chen, L. Hong, A.-L. Liu, J.-Q. Liu, X.-H. Lin and X.-H. Xia, *Talanta*, 2012, **99**, 643–648.
40 Q. Li, L. Zhang, J. Li and C. Lu, *TrAC,Trends Anal. Chem.*, 2011, **30**, 401–413.
41 S. Jiao, L. Xu, K. Jiang and D. Xu, *Adv. Mater.*, 2006, **18**, 1174–1177.
42 S.-Y. Zhang, C.-X. Fang, Y.-P. Tian, K.-R. Zhu, B.-K. Jin, Y.-H. Shen and J.-X. Yang, *Cryst. Growth Des.*, 2006, **6**, 2809–2813.
43 H. Cao, X. Qian, C. Wang, X. Ma, J. Yin and Z. Zhu, *J. Am. Chem. Soc.*, 2005, **127**, 16024–16025.
44 D. M. Wang, M. X. Gao, P. F. Gao, H. Yang and C. Z. Huang, *J. Phys. Chem. C*, 2013, **117**, 19219–19225.

45 Z. Lin, X. Dou, H. Li, Q. Chen and J.-M. Lin, *Microchim. Acta*, 2014, 1–7.
46 C. Xiao, Y. Zhang, A. Xie, Z. Wu, H. Wang and Y. Shen, *Mater. Lett.*, 2013, **111**, 51–54.
47 D. Dorfs, T. Härtling, K. Miszta, N. C. Bigall, M. R. Kim, A. Genovese, A. Falqui, M. Povia and L. Manna, *J. Am. Chem. Soc.*, 2011, **133**, 11175–11180.
48 E. J. Silvester, F. Grieser, B. A. Sexton and T. W. Healy, *Langmuir*, 1991, **7**, 2917–2922.
49 I. Kriegel, C. Y. Jiang, J. Rodriguez-Fernandez, R. D. Schaller, D. V. Talapin, E. da Como and J. Feldmann, *J. Am. Chem. Soc.*, 2012, **134**, 1583–1590.
50 Y. Bai, F. Rong, H. Wang, Y. Zhou, X. Xie and J. Teng, *J. Chem. Eng. Data*, 2011, **56**, 2563–2568.
51 M. Darouie, S. Afshar, K. Zare and M. Monajjemi, *J. Exp. Nanosci.*, 2012, **8**, 451–461.
52 P. K. Jain, X. Huang, I. H. El-Sayed and M. A. El-Sayed, *Acc. Chem. Res.*, 2008, **41**, 1578–1586.
53 J.-Z. Guo, H. Cui, W. Zhou and W. Wang, *J. Photochem. Photobiol., A*, 2008, **193**, 89–96.
54 D. M. Wang, Y. Zhang, L. L. Zheng, X. X. Yang, Y. Wang and C. Z. Huang, *J. Phys. Chem. C*, 2012, **116**, 21622–21628.
55 S. Hanaoka, J.-M. Lin and M. Yamada, *Anal. Chim. Acta*, 2000, **409**, 65–73.